Strong and Weakly Acidic OH Groups of HY Zeolite into the Different Routes of Cyclohexene Reaction: An IR Operando Study

Bruno Santos, José Zotin, Françoise Maugé, Laetitia Oliviero, Weitao Zhao, Mônica da Silva

Strong and weakly acidic OH groups of HY zeolite into the different routes of cyclohexene reaction: an IR operando study

Bruno M. Santos*[1,3], José L. Zotin[1], Françoise Maugé[2], Laetitia Oliviero[2], Weitao Zhao[2] and Mônica A. P. da Silva[3]

[1] *Centro de Pesquisas e Desenvolvimento, PETROBRAS, Rio de Janeiro (Brazil)*

[2] *Normandie Univ, ENSICAEN, UNICAEN, CNRS, LCS, 14000 Caen (France)*

[3] *Escola de Química, Centro de Tecnologia, Universidade Federal do Rio de Janeiro, Rio de Janeiro (Brazil)*

*bruno_m@petrobras.com.br

Abstract

IR operando study of cyclohexene reaction on HY zeolite (Si/Al = 15) was performed to determine the role of the OH groups located in the different zeolitic cages and the silanol groups (SiOH). A parallel between the product yield and type and amount of OH groups poisoned by coking and pyridine pulses was established. The role of silanol and zeolitic OH groups during cyclohexene conversion and the coverage rate of surface groups of the dealuminated HY zeolite, were evaluated by FT-IR operando study.

At the beginning of the reaction, zeolite exhibited a very intense deactivation due to coke formation. Coke is initially deposited on strong acid sites, inhibiting the H-transfer activity. Further, coke formation decreased. At this stage of the reaction, pyridine addition markedly decreased the isomerization activity. In parallel, it is noted that mainly SiOH, OH groups at hexagonal prisms, and perturbed OH groups in sodalite cages were mainly affected, indicating that these groups are responsible for the isomerization steps. These results showed that even weakly acidic sites are active sites for isomerization reaction.

Keywords: “operando IR”, “cyclohexene”, “isomerization”, “hydrogen transfer”, “zeolite”, “HY”, “acidity”

Graphical Abstract

In cyclohexene conversion, hydrogen transfer occurs on supercage OH groups of HY zeolite. In contrast, perturbed sodalite OH and hexagonal prisms OH, as well as SiOH groups, are responsible for isomerization steps, as revealed by pyridine pulse addition during the reaction.

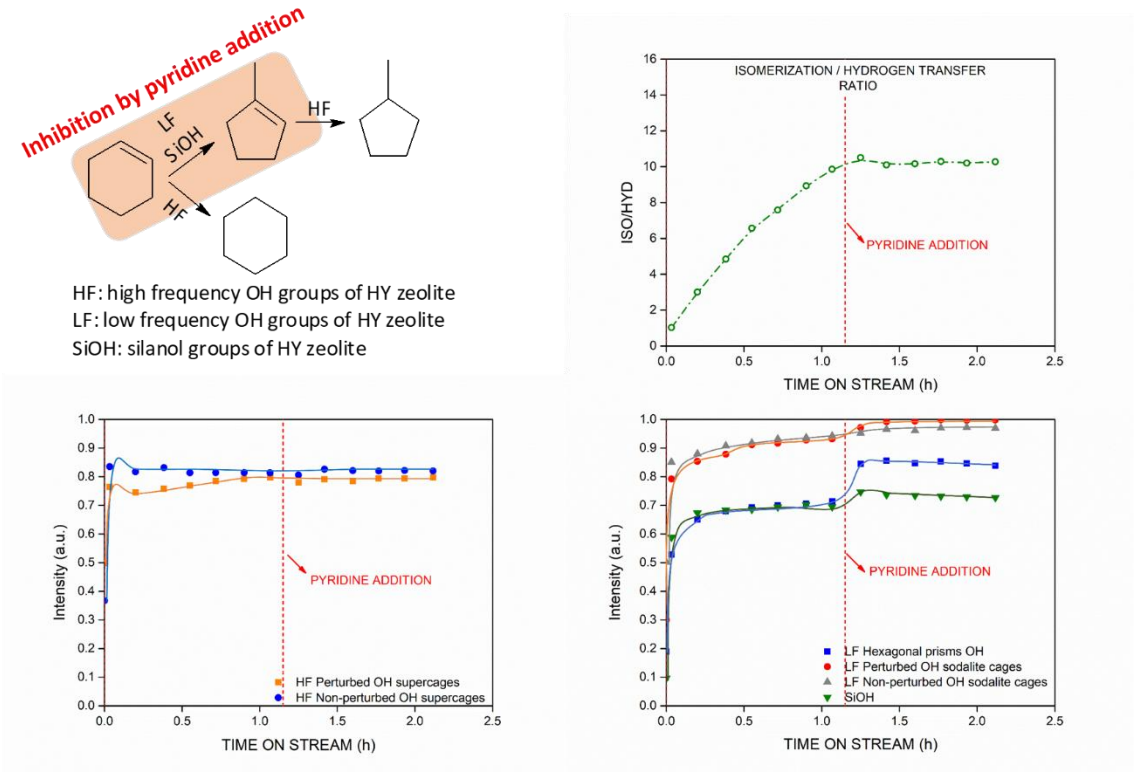

Introduction

Zeolites are widely used in petroleum industry as acid catalysts, for which the Brønsted acid sites (BAS) are usually associated with cracking and isomerization reactions. In hydrocracking processes, catalysts contain metals in addition to zeolites, which include a hydrogenation/dehydrogenation activity, resulting in bifunctional catalysts (1). Due to stringent

specifications of diesel, the incorporation of aromatic-rich streams to this fuel is limited because of their detrimental effect on density and cetane number. In this case, aromatic hydrogenation and ring-opening reactions of naphthenic compounds have been studied on bifunctional catalysts to improve such properties, which allows the processing of aromatic-rich streams to diesel fuel in refineries (2–4). Effects of support acidity on hydroprocessing catalysts were previously investigated in our research group using NiMo catalysts supported on alumina, silica-alumina or alumina-HUSY zeolite (5). The results indicated that zeolite addition increased not only isomerization and ring-opening reactions, but also hydrogenation reactions. In other work (6), it was proposed that the improvement of hydrogenation activity of zeolite-based catalysts could be associated with the formation of protonated species on zeolite acid sites, which would be easier to be hydrogenated on NiMoS sites. However, further studies of such reactions over zeolites are necessary in order to have a better understanding of this behavior.

Regarding reactions involving cyclic compounds, cyclohexene is a suitable model compound. Because it is well known as an intermediate for hydrogenation (or hydrogen transfer) reactions (7) in addition to cracking, isomerization and coke formation. Conversion of cyclohexene is extensively studied in the literature (8–16), and its reaction scheme is shown in Figure 1. Disproportioning of cyclohexene may result in cyclohexane and benzene formation by the hydrogen transfer (H-transfer) process. Additionally, coking process may also allow H-transfer reactions, forming cyclohexane; benzene formation is too low or not observed in this case. On the other hand, isomerization reactions may occur, resulting in methylcyclopentenes formation, which can be further converted to methylcyclopentane (MCP) by H-transfer reactions. It is well known in the literature that methylcyclopentenes are intermediates for ring-opening of six-ring cycles, which can be further cracked into smaller molecules depending on zeolite acidity (1).

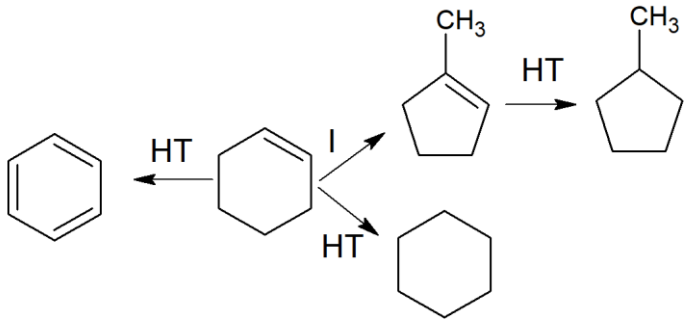

Figure 1. Pathways of cyclohexene conversion. HT: Hydrogen Transfer. I: Isomerization.

Infrared spectroscopy is one of the most widely used techniques for solid catalyst characterization. In general, catalyst properties are investigated after *in situ* activation and using probe molecules. Under working conditions, coverage of different species changes the catalyst surface, and the characterization of such species is essential to understand their role in the studied process. Operando spectroscopy is a technique that allows the observation of catalysts in such conditions (17), whose setup is available in the literature (18,19). Regarding cyclohexene conversion and n-alkane cracking in zeolites, operando spectroscopy studies have been used by several authors (18,20–25). In such works, high frequency (HF) OH groups are associated with H-transfer reactions, and they show high sensitivity to coke. Besides, HF OH groups perturbed by extraframework species, with strong Brønsted acidity, are considered active sites for cracking reactions and coke formation.

On the other hand, isomerization reactions are described as not sensitive to coke and they occur even on weak acid sites. However, the role of low frequency (LF) OH groups and silanol (SiOH) on the reaction is not well known, as well as the coverage rate of each group during the reaction. The effects of nitrogen species in the feed were also investigated in the literature. Their inhibitor effects were associated with the neutralization of BAS (26). Previous IR operando study has shown that the addition of 2,6-dimethylpyridine in the feed led to the adsorption of nitrogen species at the expense of the intermediate for alkene isomerization reaction (27), resulting in catalyst deactivation.

This work aims to evaluate, by FT-IR operando study, the coverage rate of each OH group present on HY zeolite and their role in coke formation, hydrogen transfer and isomerization steps during cyclohexene conversion.

Experimental

Catalytic tests were carried out using a stabilized HY zeolite (Zeolyst Inc., bulk Si/Al = 15, framework Si/Al = 25) with 547 m^2 g^{-1} of micropore area (measured by *t-plot* method) and specific surface area of 771 m^2 g^{-1} (measured by BET method).

Characterizations of OH groups and acidic sites were performed by FTIR spectroscopy. Each sample was pressed into a self-supported wafer (approximately 8 mg cm^{-2}) that was pre-treated in situ in the IR cell by heating from room temperature (RT) to 623 K (1 K min^{-1}), followed by an isotherm at 623 K for 1 hour under secondary vacuum (10^{-4} Pa) and a decrease to 423 K. Spectra were recorded on a Nicolet iZ10 equipped with an MCT detector, with 64 scans and 4 cm^{-1} resolution. All spectra were normalized to a constant disc mass of 500 mg cm^{-2}. Characterization of acid sites of pre-treated samples was performed by pyridine adsorption at 133 Pa and 423 K, followed by desorption at 12 Pa from 423 to 623 K at a rate of 1 K min^{-1}. Regarding band overlapping, quantification of area of each band was obtained after spectral decomposition on OMNIC 9 peak fit. The bands were adjusted considering Voigt fit analysis.

Operando study was performed in a setup previously described, consisting of a reactor cell made by stainless steel tubing, equipped with two CaF_2 windows and sealed with a Kalrez O-ring for each window (18,19,27). Samples were pressed into self-supported wafers, as described above. Prior to the tests, the zeolite was activated at 623 K for 2.5 h (heating rate of 3 K min^{-1}) under a flow of 30 mL min^{-1} of N_2. After that, the temperature was decreased to 523 K at a ramp of 3 K min^{-1}, and two different reaction tests were carried out. In the first one, defined as test 1, the reaction gas (cyclohexene and N_2 flow) was added to the cell just after the catalyst activation. In the second one, defined as test 2, the catalyst was poisoned with approximately

4.2 μmol of pyridine (at 523 K) before adding reaction gas to the cell. Then, after approximately 1.2 h of time on stream (TOS), an additional dose of 2.1 μmol of pyridine was introduced into the cell. In both tests, the temperature was 523 K, the reaction gas flow was 100 mL min^{-1} and its molar composition was 1.3% of cyclohexene and 98.7% of N_2. FTIR spectra of the catalyst surface were recorded every approximately 10 minutes on a Nicolet 6700 equipped by an MCT detector with 64 scans and 4 cm^{-1} resolution, while the composition of reactor effluent was determined by GC, utilizing a Bruker 450-GC equipment, equipped with a column BP1 50 m x 0.32 mm and a FID. Cyclohexene conversion was determined as defined in Equation (1), where $X_{cyclohexene}$ is the conversion of cyclohexene, $C_{cyclohexene}$ is the cyclohexene molar composition in effluent gas, and C_i is the molar composition of the other compounds in effluent gas.

$$X_{cyclohexene} = \left(1 - \frac{C_{Cyclohexene}}{C_{cyclohexene} + \sum_{i=1}^{n} C_i}\right) \times 100 \quad (1)$$

Product yields were calculated by Equation (2), where Y_i is the yield of product i.

$$Y_i = \frac{C_i}{\sum_{i=1}^{n} C_i} \times X_{cyclohexene} \quad (2)$$

The ratio between isomerization (1-methyl-1-cyclopentene and methylcyclopentane) and hydrogen transfer activities (cyclohexane and methylcyclopentane) was calculated according to Equation (3).

$$\frac{ISO}{HYD} = \frac{C_{1-methyl-1-cyclopentene} + C_{methylcyclopentane}}{C_{cyclohexane} + C_{methylcyclopentane}} \quad (3)$$

where ISO and HYD are the isomerization and hydrogen transfer products, respectively, and C is the molar composition of the compound indicated.

Quantification of each types of zeolitic OH groups, silanol groups, Brønsted acid sites (BAS) and Lewis acid sites (LAS), defined as η (μmol), were performed by Equation (4), where A is the IR band area, s is the area of the self-supported wafer (cm^2), and ε is the molar absorption coefficient (μmol^{-1} cm).

$$\eta = \frac{A \times s}{\varepsilon} \quad (4)$$

The coverage (Θ) of silanol and zeolitic OH groups at given TOS was calculated for each type of OH groups according to Equation (5), where the quantity corresponds to the amount of covered silanol or zeolitic OH groups (in μmol - calculated by Equation (4)). These values are obtained from the difference between the spectra taken at given TOS and the activated sample.

$$\theta = \frac{quantity\ of\ the\ OH\ group\ occupied\ at\ given\ TOS}{total\ OH\ group\ quantity\ in\ the\ HY\ zeolite} \quad (5)$$

Results and discussion

Surface sites of HY zeolite

The IR spectrum of OH groups of the activated HY zeolite and the band decomposition is shown in Figure 2. This zeolite exhibited a band corresponding to SiOH groups at 3739 cm^{-1} (28). Additionally, two bands corresponding to zeolitic high frequency (HF) OH groups were found. The first one, at 3625 cm^{-1}, was assigned to non-perturbed OH groups inside the supercages (29), and the second one, at 3606 cm^{-1}, was ascribed to perturbed OH groups inside the supercages. These latter OH groups are known as superacidic due to their interaction with the extraframework phase (30,31). Regarding low frequency (LF) OH groups, three bands were distinguished. The first one, at 3558 cm^{-1}, was assigned to non-perturbed OH groups located inside the sodalite cages (31); the second one, at 3541 cm^{-1}, corresponded to OH groups inside the sodalite cages perturbed by the extraframework phase (32), and the last one, at 3516 cm^{-1}, was attributed to OH groups in hexagonal prisms of zeolite (33). The concentration of the various groups was obtained considering a molar absorption coefficient of 7.5 μmol^{-1} cm for HF OH, 5.6 μmol^{-1} cm for LF OH (29) and 3.0 μmol^{-1} cm for SiOH (34). The results are summarized in Table 1.

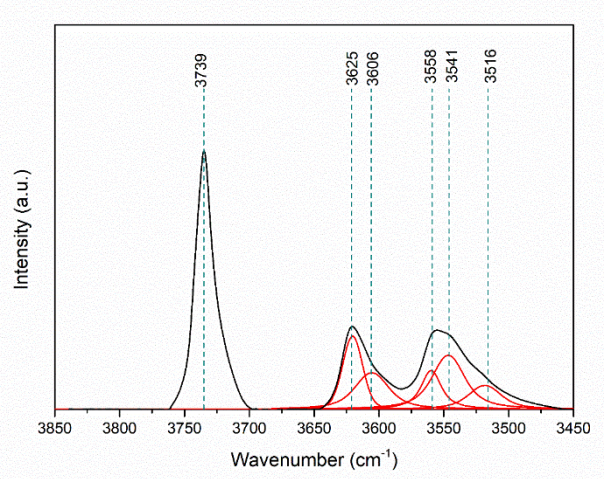

Figure 2. IR spectrum of HY zeolite in the OH region after activation at 623 K.

Table 1. Quantification of SiOH and zeolitic OH groups in HY zeolite activated at 623 K.

	IR band (attribution)	Concentration	Total	Unit
High frequency (HF) OH groups	3625 cm^{-1} (Non-perturbed OH supercages)	41	95	µmol g^{-1}
	3606 cm^{-1} (Perturbed OH supercages)	54		
Low frequency (LF) OH groups	3558 cm^{-1} (Non-perturbed OH sodalite cages)	41	176	µmol g^{-1}
	3541 cm^{-1} (Perturbed OH sodalite cages)	81		
	3516 cm^{-1} (Hexagonal prisms OH)	54		
Silanol (SiOH) groups	3739 cm^{-1} (SiOH)	524	524	µmol g^{-1}

The Brønsted (BAS) and Lewis (LAS) acidity of the HY zeolite has been probed by pyridine adsorption at 423 K and subsequent desorption by heating from the same temperature to 623 K. The obtained spectrum after pyridine desorption at 423, 523 and 623 K are shown in Figure 3 and exhibited bands at 1454 and 1621 cm^{-1}, corresponding to LAS, two bands at 1543 cm^{-1} and 1634 cm^{-1} associated with BAS, and another one related to both sites at 1490 cm^{-1}. Overall, BAS were quantified from the band area at 1543 cm^{-1} of the spectrum recorded at 423 K, considering a molar absorption coefficient of 1.8 μmol^{-1} cm (29). In contrast, overall, LAS were determined from the area of the band at 1454 cm^{-1} in the same spectrum, with a molar absorption coefficient of 1.5 μmol^{-1} cm (35). The resulting values obtained were 200 $\mu mol\ g^{-1}$ of BAS and 140 $\mu mol\ g^{-1}$ of LAS. Spectra recorded at 523 and 623 K exhibit the BAS and LAS with higher strength. At 523 K, zeolite presented 170 $\mu mol\ g^{-1}$ of BAS and 105 $\mu mol\ g^{-1}$ of LAS and, at 623 K, were found 99 $\mu mol\ g^{-1}$ and 78 $\mu mol\ g^{-1}$ of BAS and LAS, respectively, indicating that approximately half of BAS and LAS on the zeolite are very strong sites.

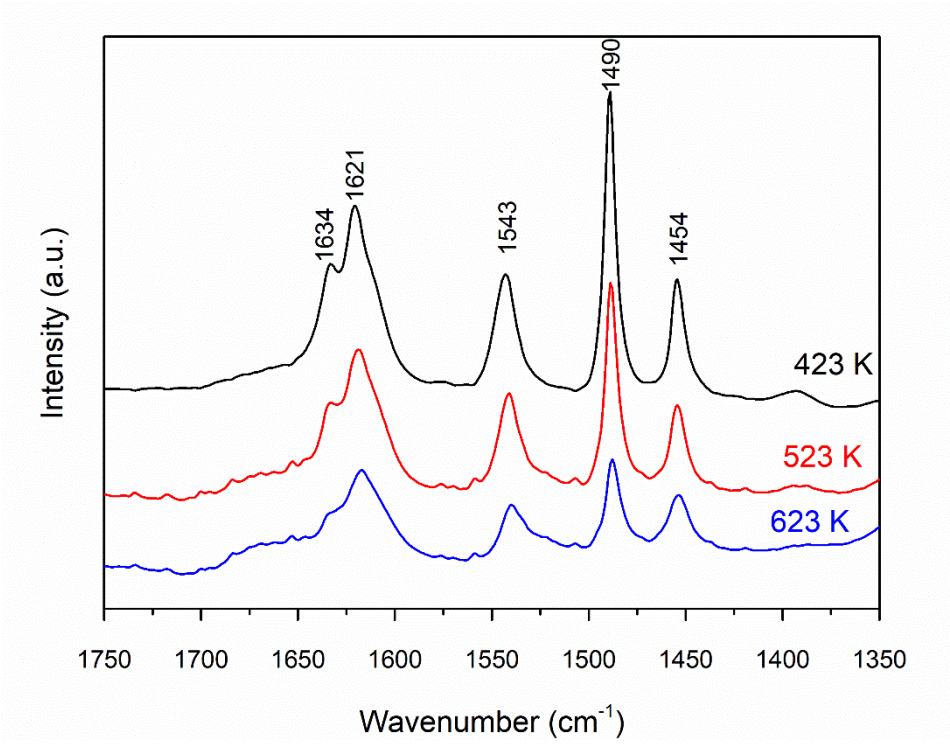

Figure 3. IR spectrum of pyridine after desorption at 423 K, 523 K and 623 K over HY zeolite.

Operando IR study during cyclohexene reaction

The reaction of cyclohexene on HY zeolite was followed in operando by FTIR spectroscopy and GC, simultaneously. As for test 1, cyclohexene conversion (X), product yield (Y), and ISO/HYD ratio are shown in Figures 4a and b. The main products formed were 1-methyl-1-cyclopentene, methylcyclopentane (MCP) and cyclohexane.

Cyclohexene conversion and coke formation

The results indicated a rapid decrease in catalyst activity (Figure 4a) in the first 0.2 h, followed by a smaller one at greater TOS.

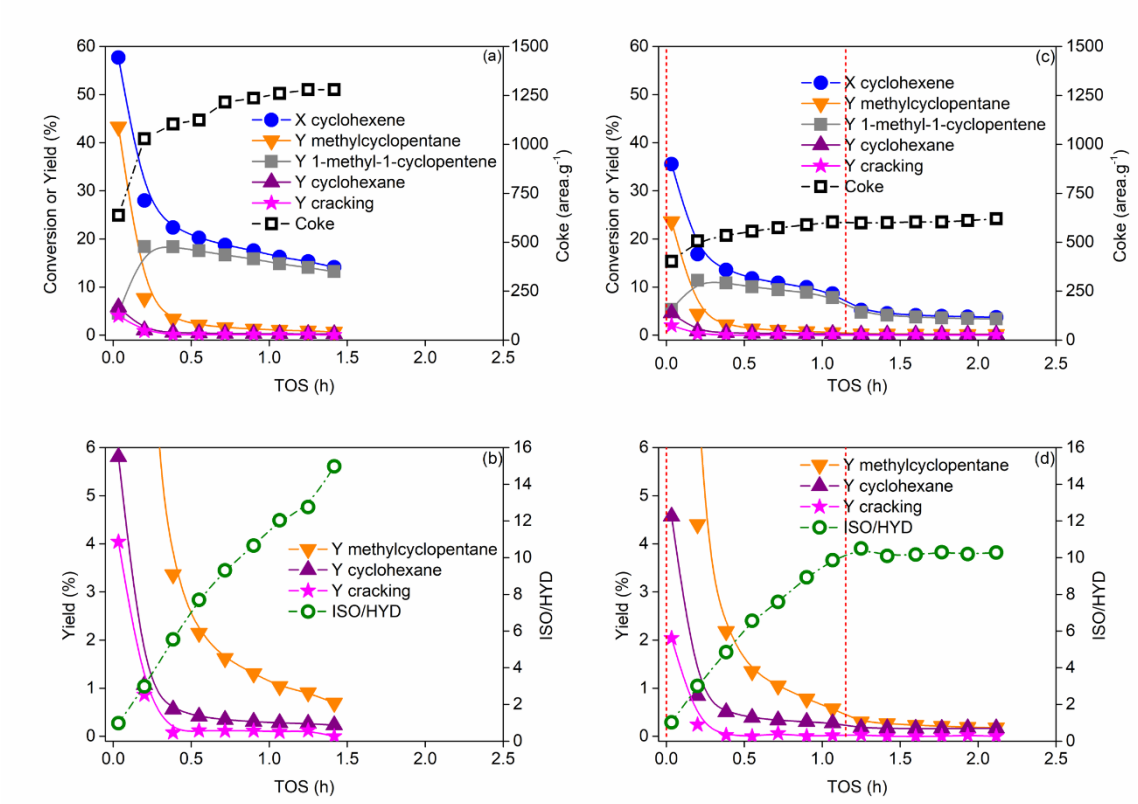

Figure 4. Catalytic data observed in Test 1 (a and b) and Test 2 (c and d). Graphs a and c present the cyclohexene conversion, product yield and coke deposition. Graphs b and d present

ISO/HYD ratio and amplified scale of cyclohexane, methylcyclopentane and cracking yields (also shown in a and c). Dashed red line indicates the second pyridine poisoning in test 2.

Meanwhile, coke deposition was evidenced. On the IR spectrum taken after 10 min in test 1 (Figure 5A), bands related to coke (~1591, 1379 and 1348 cm^{-1}) were observed. According to Jolly *et al.* (20), the band at 1591 cm^{-1} is associated with graphitic coke, while the band at 1348 cm^{-1} refers to pre-graphitic carbons. Additionally, a band was found at 1496 cm^{-1} that can be associated with unsaturated carbenium ions (18,36), an intermediate of cyclohexene reaction through H-transfer (21). The band at 1450 cm^{-1} was referred to as a combination of contributions from adsorbed intermediate species and coke (18,21). The amount of deposited coke during the reaction was estimated according to the intensity of the 1591 cm^{-1} band, as reported in Figure 4a. Thus, fast coke deposition was evidenced in the first 0.2 h of operation and then coke formation became smaller, with a small change in slope at approximately 0.7 h. Evolution of coke with TOS is inversely parallel to the cyclohexene conversion.

To understand the origin of the rapid initial deactivation, a second test (test 2) was carried out in which the zeolite was previously contacted with 4.2 μmol of pyridine in order to selectively poison the strong acid sites and observe the catalyst behavior in terms of sites coverage, activity and selectivity. Figure 5 (B and C) compares the surface species after initial pyridine addition in test 2, as well as after the subsequent 10 minutes of TOS in both tests. The spectrum taken before the reaction in test 2 (Figure 5B) presents the same pyridine bands as already described in Figure 3. The quantity of BAS and LAS initially poisoned in test 2 was then determined to be 62 μmol g^{-1} (31% of total BAS) and 23 μmol g^{-1} (17% of total LAS), respectively.

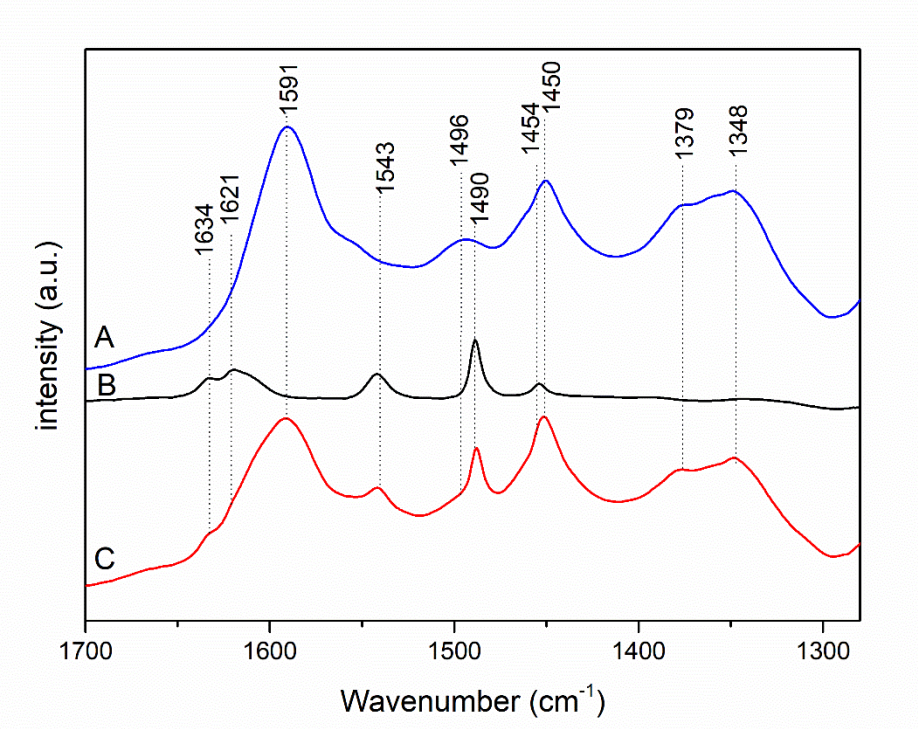

Figure 5. IR spectra of HY before and during cyclohexene reaction. A: spectrum taken in test 1, after 10 minutes of reaction; B: spectrum taken in test 2, after pyridine addition and before reaction; C: spectrum taken in test 2, after pyridine addition and 10 minutes of subsequent reaction.

After 10 min of reaction in test 2, the bands associated with coke were observed in addition to those related to pyridine species, already present on the sample before reaction (Figure 5C). However, bands of pyridine species at 1454 cm^{-1} and 1490 cm^{-1} were very close to the ones related to the adsorption of intermediate species of cyclohexene reaction. It can be noted that globally the intensity of the IR bands at 1348, 1379 and 1591 cm^{-1} was lower in test 2 than in test 1, showing that the initial poisoning by pyridine has decreased the coke formation during the first 10 min of reaction. Meanwhile, the initial cyclohexene conversion is lower in test 2 than in test 1 (Figures 4a and c)

In test 2, after 1.2 h of TOS, a second pyridine pulse was injected. IR spectra taken before (B) and after (A) the new pyridine introduction are shown in Figure 6. The bands typical of coke

were observed at 1591, 1379 and 1348 cm^{-1}, *i.e.*, at very close wavenumbers as in Figure 5. One can note the absence of the band at 1496 cm^{-1} related to intermediate species of cyclohexene reaction through H-transfer. This inobservance agrees with the low amount of hydrogen transfer products formed after 1.2 h. The subtracted spectrum (Figure 6 (A-B)) showed a small decrease of the coke band at 1591 cm^{-1} that is very limited compared to the overall intensity of the band, as was also observed by Jolly *et al.* (23). This could be ascribed to a limited desorption of coke by pyridine adsorption.

Besides, the second pulse led to pyridine band appearance similar to those observed previously, although with a weaker intensity. Amounts of BAS and LAS poisoned by this second pyridine injection were calculated from (A-B) spectrum and corresponded to 16 and 17 µmol g^{-1}, respectively.

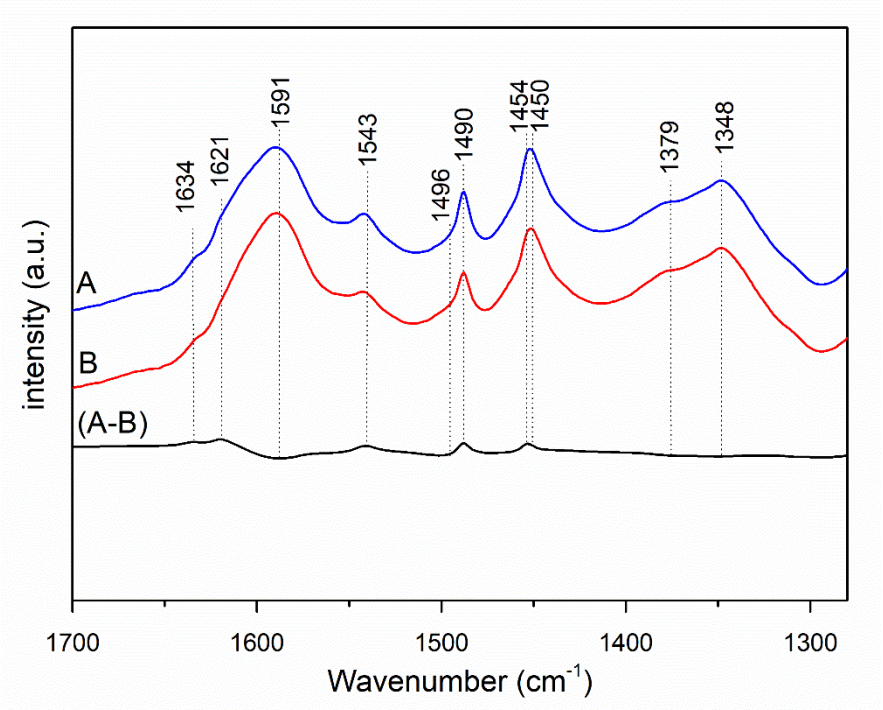

Figure 6. IR spectra of HY during cyclohexene reaction (test 2). Spectrum taken before (B) and after (A) second pyridine addition at TOS = 1.2 h, and the difference spectrum (A-B).

Selectivity changes with TOS

The selectivity of the reaction was followed for tests 1 and 2 (Figures 4a and c). At the beginning of test 1, the high formation of methylcyclopentane decreased very fast, while the formation of 1-methyl-1-cyclopentene increased. After that, 1-methyl-1-cyclopentene yield decreased very slowly, while methylcyclopentane yield became very small and coke formation moderately increased. The behaviors followed by cyclohexane and cracking products were similar to that of methylcyclopentane, but their yields are very small. Figure 4b points out that methylcyclopentane formation was greater than that of cyclohexane, as well as its deactivation. As a result of these evolutions, ISO/HYD ratio increased continuously with TOS, indicating a higher deactivation of hydrogen transfer than isomerization activity with TOS.

Evolution of product yields and ISO/HYD ratio for test 2 are shown in Figures 4c and d. Comparison with test 1 shows that the first dose of pyridine, introduced before test 2, initially resulted in a lower cyclohexene conversion but that the nature of the main products, as well as their evolution with TOS and the ISO/HYD ratio during the first hour of reaction were similar to test 1.

The second addition of pyridine, performed at approximately 1.2 h (indicated by a red line in Figures 6c and d), led to a supplementary decrease of cyclohexene conversion. This can be explained by competition between pyridine species and cyclohexene reaction intermediates for the acid sites. It should be noted that ISO/HYD ratio stabilized after the second dose of pyridine. Regarding product yields, 1-methyl-1-cyclopentene presented the highest deactivation, methylcyclopentane suffered a decrease in its yield, likely related to the 1-methyl-1-cyclopentene formation decrease, and the effect on cyclohexane formation was very low. Therefore, after the second pyridine poisoning, isomerization activity was more affected than hydrogen transfer.

Evolution of the coverage rate of hydroxyl groups with TOS

The IR spectra obtained in the operando study allows to follow not only the coke deposition and intermediate species formation on the catalyst surface but also interestingly the coverage of hydroxyl groups during the reaction. Hence, the coverage rate (fraction of occupied hydroxyl groups calculated from Equation 5) of SiOH and zeolitic OH groups during test 1 is shown in Figures 7a and b, respectively. Regarding HF OH groups (Figure 7a), the non-perturbed OH groups inside the supercages (3625 cm^{-1}) were covered almost instantaneously and remained so during the test. In contrast, the perturbed OH groups inside the supercages (3606 cm^{-1}) also presented a strong coverage at the beginning of the reaction and showed some small coverage modification with TOS. Indeed, a slight recovery is first noted, and further, a small coverage increase occurred throughout the reaction.

Regarding LF OH groups (Figure 7b), the coverage of the non-perturbed OH groups inside the sodalite cages (3558 cm^{-1}) was almost instantaneous and complete and remained stable during the test. Otherwise, the perturbed OH groups inside the sodalite cages (3541 cm^{-1}) also presented a strong initial coverage, although lower, that is followed by a progressive increase with TOS. Then, both OH groups at hexagonal prisms (3516 cm^{-1}) and SiOH groups (3739 cm^{-1}) exhibited similar behavior with gradual coverage during TOS. Besides, Figure 7b revealed a slightly more marked coverage at approximately 0.7 h for all groups. At the end of the test, only the LF OH groups inside sodalite cages (perturbed and non-perturbed) were fully covered (coverage near to 1).

After 1.4 h of the test, the cyclohexene flow was cut off. The catalyst was maintained under inert gas flow in order to distinguish the coverage due to the adsorption of intermediate species from that due to coke. The results are shown in Online Resource 1 (S1). The coke species remained constant. In contrast, the intermediate species decreased but did not disappear, indicating that the sites remained covered due to a combination of coke and intermediate species with strong interaction. In parallel, after cyclohexene flow cutting off, only the OH groups in

the hexagonal prisms and SiOH groups presented a decrease of coverage, which indicates the release of weakly intermediate adsorbed species. By contrast, the other groups remained covered by coke.

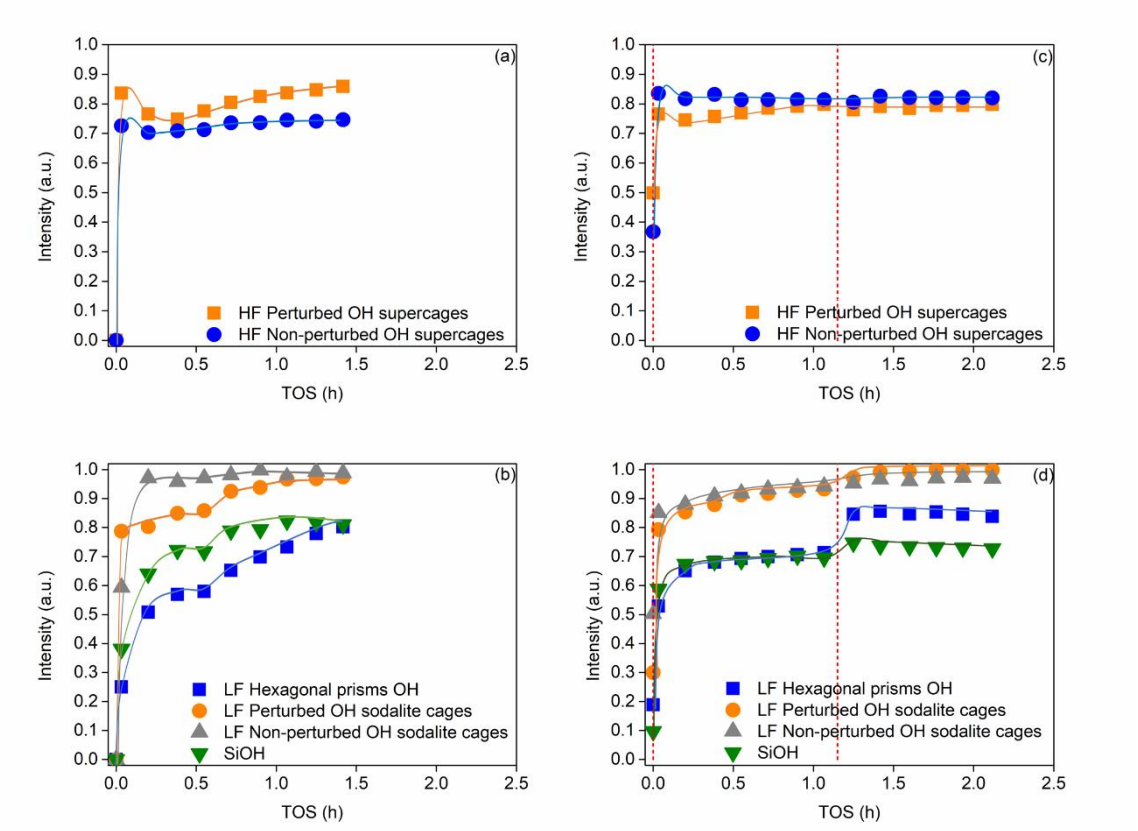

Figure 7. Coverage rates of the HY zeolite OH group during Test 1 (a and b) and Test 2 (c and d) versus TOS. HF OH groups (a and c) LF OH and SiOH groups (b and d).

The coverage of zeolitic OH groups and SiOH groups in test 2 is shown in two ways to distinguish the TOS effect from that of the pyridine addition effect. The concentrations of occupied groups after the first pyridine poisoning (before the reaction), as well as before and after the second pyridine dose, are listed in Table 2. Besides, the coverage during the reaction is displayed in Figure 7c and d.

After the first pyridine poisoning, the concentration of poisoned perturbed supercage OH groups was higher than that of non-perturbed ones (Table 2, Figure 7c). As for LF OH groups, the quantity of poisoned perturbed sodalite cage OH groups was almost similar to that of non-perturbed ones. In contrast, the quantity of OH groups located at hexagonal prisms poisoned by pyridine was smaller (Figure 7d). Silanol groups presented the lowest poisoning by pyridine since only approximately 10% of such groups were in interaction with pyridine (Figure 7d).

At this initial step, pyridine adsorbed on the strongest acid sites of the zeolite. So, the results regarding the poisoning of HF groups are consistent with those reported in previous works (30,31), where perturbed HF groups of HY zeolite are considered superacidic. The smaller difference observed between the poisoning of perturbed and non-perturbed groups in sodalite cages could be associated with the lower accessibility to pyridine of such groups (32).

Table 2. Concentration of HY acidic sites poisoned by first and second pyridine addition in Test 2.

		Unit	After 1st poisoning	Before 2nd poisoning	After 2nd poisoning
TOS		h	0	1.1	1.3
High frequency OH	Non-perturbed OH supercages	µmol g^{-1}	15	34	33
	Perturbed OH supercages	µmol g^{-1}	27	43	42
Low frequency OH	Non-perturbed OH sodalite cages	µmol g^{-1}	21	39	39
	Perturbed OH sodalite cages	µmol g^{-1}	25	78	81

Hexagonal prisms OH	µmol g^{-1}	10	38	45
SiOH groups	µmol g^{-1}	51	364	391
BAS	µmol g^{-1}		62	78*
LAS	µmol g^{-1}		23	40*

* Sum of poisoned sites at first and second doses of pyridine

For test 2, the evolution of coverage rates between the first and second doses of pyridine (left of the red line in Figure 7c and d) revealed the impact of the interaction with reactants and products as well as coking. Thus, comparing the OH group coverages between tests 1 and 2 allowed determining the impact of pyridine poisoning. Hence, except HF OH groups, all OH groups presented a lower coverage after 1.2 h of reaction in test 2 than in test 1, which could be directly linked to the lower coke formation. Accordingly, the initial blockage of the stronger acidic sites by pyridine adsorption inhibits coke formation and leads to a lower OH group poisoning by coke in reaction conditions.

The second dose of pyridine (right of the red line in Figures 7c and d) increased the coverage with TOS for SiOH, OH groups at hexagonal prisms and perturbed OH groups in sodalite cages (this last one was fully covered after this second pulse). Interestingly, it did not impact the coverage of both supercage OH groups and non-perturbed sodalite cage OH groups that kept coverages of 80% and 95%, respectively.

Deactivation process

The fast deactivation process identified at the beginning (up to 0.2 h) of the tests 1 and 2 can be associated with the reduction of hydrogen transfer reactions since methylcyclopentane and cyclohexane were the products that suffered the highest decrease in their formation. Hence, hydrogen transfer reactions are more affected by fast coke formation than isomerization reactions, as was reported by Joly *et al.* (18). Coke formation has a dual impact. Indeed, it blocks the active sites for H-transfer reactions, but coke formation is also a source of hydrogen, allowing a hydrogenation activity in the absence of H_2 in the flow.

After this initial stage, a slow deactivation stage occurred. This was associated with the decrease of 1-methyl-1-cyclopentene formation and that could be ascribed to the increase of "slow" coke. However, ISO/HYD ratio continuously increased. This can be explained by the higher deactivation of hydrogen transfer reactions, more dependent on the coking process than isomerization. Indeed, a decrease in coke formation made hydrogen availability more limited. Thus, hydrogen transfer reactions are decreased, favoring 1-methyl-1-cyclopentene formation. These observations are consistent with the fact that hydrogen transfer reactions are more sensitive to coke than isomerization reactions, as reported by Joly *et al.* (18). Finally, considering the H-transfer products and reaction scheme shown in Figure 1, the conversion of 1-methyl-1-cyclopentene to methylcyclopentane was the preferential route at the expense of the direct formation of cyclohexane, indicating that cyclohexene is preferentially isomerized before H-transfer step.

One can also note a small coke amount increase at 0.7 h of TOS. One could note that a decrease of intermediate species band intensity, shown in Online Resource 1 (S2), was observed at the same TOS. This is in accordance with previously reported work (18), where a decrease of such species was associated with the stabilization of coke. Also, in parallel, a slope change in the coverage rate of SiOH and LF OH groups occurred, as shown in Figure 7b, indicating that the additional coke was formed on such sites.

Active sites for the various pathways of cyclohexene reaction

Figures 7c and d showed that, in test 2, the first introduction of pyridine (before the reaction) led to a perturbation of all OH group types. Nevertheless, the interaction with supercage OH groups and non-perturbed sodalite OH groups is more marked. The interaction is maximum with the supercage perturbed OH groups (50%) that with the non-perturbed ones (37%) (Figure 7c). As a consequence of the smaller amount of available acid sites, the initial conversion was clearly lower in test 2 (36%) than in test 1 (58%). Comparison between tests 1 and 2 (Figures 4a and c) reveals that pyridine poisoning did not affect 1-methyl-1-cyclopentene yield (~5%), while methylcyclopentane yield sharply decreased (from 43% in test 1 to 24% in test 2). This allows concluding the hydrogen transfer required strongly acidic zeolitic OH groups. Meanwhile, the ISO/HYD ratio was similar for tests 1 and 2 at the beginning of the reaction. This suggests that initial addition of pyridine blocked the same sites as "fast" coke species.

After the second dose of pyridine (test 2), a supplementary decrease of cyclohexene conversion was observed (Figure 4c). In parallel, Figure 7d showed an increase in the poisoning of the weakly acidic sites as silanol, OH groups in hexagonal prisms and perturbed sodalite cage OH groups. At this stage, no supplementary poisoning of the more acidic species (HF OH species and non-perturbed sodalite cage) were detected. It can be mentioned that these species were already strongly poisoned either by the first pyridine pulse or by coke formed with TOS, although not completely poisoned (80-95% - Figures 7c and d). It was also noticeable that the second pyridine pulse markedly affected the ISO/HYD ratio (Figure 4d). Indeed, the ratio stopped its increase with TOS and became constant. Besides, the second pyridine pulse led to a decrease of 1-methyl-1-cyclopentene yield (isomerization product). The decrease of methylcyclopentane yield observed was likely a consequence of the low amount of 1-methyl-1-cyclopentene formed. The other products whose yield was very low were almost unaffected. Thus, one can conclude that SiOH, OH groups in hexagonal prisms and sodalite cages perturbed OH groups are involved in the isomerization route.

Regarding SiOH groups, test with pure silica (shown in Online Resource 1, S3) revealed that such groups are inactive for cyclohexene reactions. However, it is known that the presence of a small amount of Al into silica generates Brønsted acid sites and can give a substantial activity to silica (37,38). This could explain the activity in cyclohexene isomerization of the silanol groups of the zeolite.

On the other hand, the second pyridine addition did not influence hydrogen transfer reactions nor the coverage of supercage OH groups, confirming that such groups are responsible for hydrogen transfer reactions. More specifically, according to other authors (39), HF OH groups perturbed by extraframework Al species are responsible for such reactions because neighboring Al sites are required to facilitate hydrogen transfer between sorbed carbenium ions and alkenes.

Lewis acid sites related to the extraframework Al content in the zeolite (40,41) were also poisoned by pyridine. However, no direct association between the poisoning of such sites and product distribution was found, as reported by others (23).

Coke formation

A lower coke amount was formed in test 2 than in test 1. It can be associated with the poisoning of the strongest acid sites of HY catalyst by the initial pyridine pulse in test 2. This agrees with previous work (21), which showed that coking process depends on initial BAS concentration and is favored by strong acid sites. However, it should be noted that only limited changes in the evolution of coverage of OH groups in supercages and sodalite cages occurred between the two tests. Then, comparing the coverages at the end of the test without pyridine (test 1) and before the second pyridine poisoning (test 2), significantly lower coverage of SiOH and OH groups at hexagonal prisms is observed in the presence of pyridine. The evolution of coverage of OH groups in hexagonal prims occurred continuously in test 1, while in test 2, it increased more rapidly and achieved a limit value after 0.2h. These behaviors agree with the evolution of coke formation during both tests. Based on these results, coke deposition initially occurred on the

strong acid sites, which promoted an intense deactivation at the beginning. After that, the slow and limited deactivation rate observed was attributable to coke deposition on OH groups with lower acidity as SiOH, non-perturbed sodalite cage OH groups and OH groups in hexagonal prisms.

One point to mention is that the coverage rate of supercage OH groups is never complete (Figure 7) whereas OH groups inside sodalite cages can be fully covered after 1.5 h of reaction. As mentioned before, the coverage of these groups remained after cutting off cyclohexene feed, indicating that they were irreversibly poisoned by coke. Thus, one possible reason for the partial coverage of supercage OH groups could be related to the blockage of the accessibility of such groups by coke.

Conclusions

This IR operando study allows to highlight the role of the various acidic OH groups of HY zeolite for the different pathways of cyclohexene transformation reaction. Parallel between the type and amount of OH groups poisoned by coking or by different pyridine pulses and the reaction product yields were performed.

First fast and then slow deactivation occurred during cyclohexene reaction. The fast coke formation mostly poisoned the stronger acidic sites of HY, *i.e.*, perturbed and non-perturbed supercage OH groups and non-perturbed sodalite cages ones. In parallel, a strong decrease in H-transfer activity is observed. Similarly, the introduction of pyridine before the reaction that led to preferential poisoning of the stronger acid sites also decreased the methylcyclopentane and cyclohexane yields. This showed that these strongly acidic OH groups are responsible for H-transfer activity.

During the slow deactivation stage, a decrease of the 1-methyl-1-cyclopentene yield occurred. After one hour of reaction, the introduction of a pyridine pulse led to a marked decrease of the isomerization product and stabilized the ISO/HYD ratio at a constant value. Simultaneously,

specific poisoning of the silanol and zeolitic hexagonal prism and perturbed sodalite cage OH groups was observed. This led to the conclusion that these weakly acidic sites are active sites for isomerization reaction.

These findings contributed to a complete understanding of the HY zeolite behavior during the cyclohexene reaction. They will support further studies on the evaluation of the role of metals, such as Ni and Mo, into zeolite, which are present in hydrocracking catalysts.

Acknowledgments

The authors would like to thank Dr. Philippe Bazin for the support in the pyridine adsorption experiments and operando setup development, as well as Dr. Alexandre Vimont and Yoann Levaque. The authors are also grateful to PETROBRAS and LCS for the financial support and the authorization for using the facilities for carrying out the experiments.

Conflict of interest

The authors declare that they have no conflict of interest.

References

1. Du H, Fairbridge C, Yang H, Ring Z. The chemistry of selective ring-opening catalysts. Appl Cat A. 2005;294(1):1–21.

2. McVicker G, Daage M, Touvelle M, Hudson CW, Klein DP, Baird Jr M, et al. Selective Ring Opening of Naphthenic Molecules. J Catal. 2002;210(1):137–48.

3. Santana R, Do P, Santikunaporn M, Alvarez W, Taylor J, Sughrue E, et al. Evaluation of different reaction strategies for the improvement of cetane number in diesel fuels. Fuel. 2006;85(5–6):643–56.

4. Stanislaus A, Marafi A, Rana MS. Recent advances in the science and technology of ultra low sulfur diesel (ULSD) production. Catal Today. 2010;153(1–2):1–68.

5. Ferraz SGA, Zotin FMZ, Araujo LRR, Zotin JL. Influence of support acidity of NiMoS catalysts in the activity for hydrogenation and hydrocracking of tetralin. Appl Cat A. 2010;384(1–2):51–7.

6. Ferraz SGA, Santos BM, Zotin FMZ, Araujo LRR, Zotin JL. Influence of Support Acidity of NiMo Sulfide Catalysts for Hydrogenation and Hydrocracking of Tetralin and Its Reaction Intermediates. Ind Eng Chem Res. 2015;54(10):2646–56.

7. Cheng WC, Rajagopalan K. Conversion of cyclohexene over Y-zeolites: A model reaction for hydrogen transfer. J Catal. 1989;119(2):354–8.

8. Aboul-Gheit AK, Aboul-Fotouh SM, Aboul-Gheit NAK. Effect of combining palladium, iridium or rhenium with platinum supported on H-ZSM-5 zeolite on their cyclohexene hydroconversion activities. Appl Catal A Gen. 2005;292:144–53.

9. Romero-Rivera R, Delvalle M, Alonso G, Flores E, Castillon F, Fuentes S, et al. Cyclohexene hydrogenation with molybdenum disulfide catalysts prepared by ex situ decomposition of ammonium thiomolybdate-cetyltrimethylammonium thiomolybdate mixtures. Catal Today. 2008;130(2–4):354–60.

10. Vít Z, Gulkova D, Kaluza L, Zdrazil M. Synergetic effects of Pt and Ru added to Mo/AlO sulfide catalyst in simultaneous hydrodesulfurization of thiophene and hydrogenation of cyclohexene. J Catal. 2005;232(2):447–55.

11. des Rochettes BM, Marcilly C, Gueguen G, Bousquet J. Kinetic study of hydrogen transfer of olefins under catalytic cracking conditions. Appl Catal. 1990;58:35–52.

12. Dwyer J, Karim K, Ojo AF. Bimolecular hydrogen transfer over zeolites and SAPOs having the faujasite structure. J Chem Soc Faraday Trans. 1991;87(5):783–96.

13. Li P, Liu X, Zhang C, Chen Y, Huang B, Liu T, et al. Selective hydrodesulfurization of gasoline on Co/MoS 2±x catalyst: Effect of sulfur defects in MoS 2±x. Appl Catal A Gen. 2016;524:66–76.

14. Bukin KA, Potapenko O V, Doronin VP, Sorokina TP, Gulyaeva TI. Performance of a zeolite-containing catalyst and catalysts based on noble metals in intermolecular hydrogen transfer between C6 hydrocarbons. Kinet Catal. 2017;58(3):271–8.

15. Boudart M, McConica CM. Catalytic hydrogenation of cyclohexene. J Catal. 1989;117:33–41.

16. Soto-Puente M, Del Valle M, Flores-Aquino E, Avalos-Borja M, Fuentes S, Cruz-Reyes J. Synthesis, characterization and cyclohexene hydrogenation activity of high surface area molybdenum disulfide catalysts. Catal Lett. 2007;113(3–4):170–5.

17. Alayoglu S, Somorjai GA. Nanocatalysis II: In Situ Surface Probes of Nano-Catalysts and Correlative Structure–Reactivity Studies. Catal Lett. 2015;145(1):249–71.

18. Joly JF, N.Zanier-Szydlowski, Colin S, Raatz F, Saussey J, Lavalley JC. Infrared in situ characterization of HY zeolite acid sites during cyclohexene transformation. Catal Today. 1991;9:31–8.

19. Lesage T, Verrier C, Bazin P, Saussey J, Daturi M. Studying the NOx-trap mechanism over a Pt-Rh/Ba/Al2O3catalyst by operando FT-IR spectroscopy. Phys Chem Chem

Phys. 2003;5(20):4435–40.

20. Jolly S, Saussey J, Lavalley JC, Zanier N, Benazzi E, Joly JF. in Situ Ft-Ir Study of Acid Sites Responsible for Cyclohexene Conversion on Hy Zeolites. Proc 9th Int Zeol Conf. 1993;319–26.

21. Jolly S, Saussey J, Lavalley LC, Zanier N, Benazzi E, Joly JF. The effect of 2,6-dimethylpyridine poisoning on the activity in n-hexane cracking of dealuminated HY zeolites. Ber Bunsenges Phys Chem. 1993;97(3):313–5.

22. Jolly S, Saussey J, Lavalley JC. FT-IR characterization of carbenium ions, intermediates in hydrocarbon reactions on H-ZSM-5 zeolites. Catal Lett. 1994;24(1–2):141–6.

23. Jolly S, Saussey J, Lavalley LC. FT-IR study of hydrocarbon conversion on dealuminated HY zeolites in working conditions. J Mol Catal. 1994;86:401–21.

24. Li H, Kadam SA, Vimont A, Wormsbecher RF, Travert A. Monomolecular Cracking Rates of Light Alkanes over Zeolites Determined by IR Operando Spectroscopy. ACS Catal. 2016;6(7):4536–48.

25. Kadam SA, Li H, Wormsbecher RF, Travert A. Impact of Zeolite Structure on Entropic–Enthalpic Contributions to Alkane Monomolecular Cracking: An IR Operando Study. Chem Eur J. 2018;24:5489–92.

26. Mendes PSF, Silva JM, Ribeiro MF, Bouchy C, Daudin A. Quantification of the available acid sites in the hydrocracking of nitrogen-containing feedstocks over USY shaped NiMo-catalysts. J Ind Eng Chem. 2019;71:167–76.

27. Travert A, Maugé F. IR study of hydrotreating catalysts in working conditions: comparison of the acidity present on the sulfided phase and on the alumina support. In: Delmon B, Froment GF, Grange P, editors. Hydrotreating and Hydrocracking of Oil Fractions. Amsterdam: Elsevier; 1999. p. 269–77.

28. Gabrienko AA, Danilova IG, Arzumanov SS, Pirutko L V, Freude D, Stepanov AG.

Direct Measurement of Zeolite Brønsted Acidity by FTIR Spectroscopy: Solid-State 1H MAS NMR Approach for Reliable Determination of the Integrated Molar Absorption Coefficients. J Phys Chem C. 2018;122(44):25386–95.

29. Khabtou S, Chevreau T, Lavalley JC. Quantitative infrared study of the distinct acidic hydroxyl groups contained in modified Y zeolites. Microporous Mater. 1994;3:133–48.

30. Malicki N, Beccat P, Bourges P, Fernandez C, Quoineaud AA, Simon LJ, et al. A new model for acid sites in dealuminated Y zeolites. Vol. 170, Stud. Surf. Sci. Catal. Elsevier B.V.; 2007. 762–770 p.

31. Vimont A, Thibault-Starzyk F, Daturi M. Analysing and understanding the active site by IR spectroscopy. ChemSoci Rev. 2010;39(12):4928–50.

32. Thibault-Starzyk F, Maugé F. Infrared Spectroscopy. In: Che M, Védrine JC, editors. Characterization of SolidMaterials and Heterogeneous Catalysts: From Structure to Surface Reactivity. Wiley-VCH Verlag GmbH & Co; 2012.

33. Long J, Wang X, Ding Z, Xie L, Zhang Z, Dong J, et al. Cyclopentadiene transformation over H-form zeolites : TPD and IR studies of the formation of a monomeric cyclopentenyl carbenium ion intermediate and its role in acid-catalyzed conversions. J Catal. 2008;255:48–58.

34. Gallas JP, Lavalley JC, Burneau A, Barres O. Comparative study of the surface hydroxyl groups of fumed and precipitated silicas. 4. Infrared study of dehydroxylation by thermal treatments. Langmuir. 1991 Jun;7(6):1235–40.

35. Hadjiivanov K. Identification and Characterization of Surface Hydroxyl Groups by Infrared Spectroscopy. Adv Catal. 2014;57:99–318.

36. Paweewan B, Barrie PJ, Gladden LF. Coking and deactivation during n-hexane cracking in ultrastable zeolite Y. Appl Catal A. 1999;185(2):259–68.

37. West PB, Haller GL, Burwell RL. The catalytic activity of silica gel. J Catal.

1973;29(3):486–93.

38. Crépeau G, Montouillout V, Vimont A, Mariey L, Cseri T, Maugé F. Nature, structure and strength of the acidic sites of amorphous silica alumina: An IR and NMR study. J Phys Chem B. 2006;110(31):15172–85.

39. Pine LA, Maher PJ, Wachter WA. Prediction of cracking catalyst behavior by a zeolite unit cell size model. J Catal. 1984 Feb 1;85(2):466–76.

40. Liu C, Li G, Hensen EJM, Pidko EA. Nature and Catalytic Role of Extraframework Aluminum in Faujasite Zeolite: A Theoretical Perspective. ACS Catal. 2015;5(11):7024–33.

41. Maache M, Janin A, Lavalley JC, Joly JF, Benazzi E. Acidity of zeolites Beta dealuminated by acid leaching: An FTIR study using different probe molecules (pyridine, carbon monoxide). Zeolites. 1993;13:419–26.